The Multi-dimensional Phase Unwrapping Integral and Applications to Microwave Tomographical Image Reconstruction

Qianqian Fang, Paul M. Meaney, *Member, IEEE,* Keith D. Paulsen, *Member, IEEE,*

***Abstract*— Spatial unwrapping of the phase component of time varying electromagnetic fields has important implications in a range of disciplines including synthetic aperture radar (SAR) interferometry, MRI, optical confocal microscopy and microwave tomography. This paper presents a fundamental framework based on the phase unwrapping integral, especially in the complex case where phase singularities are enclosed within the closed path integral. With respect to the phase unwrapping required when utilized in Gauss-Newton iterative microwave image reconstruction, the concept of dynamic phase unwrapping is introduced where the singularity location varies as a function of the iteratively modified property distributions. Strategies for dynamic phase unwrapping in the microwave problem were developed and successfully tested in simulations and clinical experiments utilizing large, high contrast targets to validate the approach.**

***Index Terms*— Phase Unwrapping, Scattering Null, Phase Singularity, Microwave Imaging**

I. Introduction

The complex notation is used in many physical problems to simplify the associated mathematics into succinct expressions, especially when analyzing wave phenomena in the frequency domain. The magnitude and phase are often convenient representations because many physical quantities can be measured and processed directly in this form. Consequently, understanding the magnitude and phase in both the mathematical and physical context is important. In this paper we focus primarily on the phase which is most often the more difficult quantity to process.

In many applications, the phase of a signal encodes rich temporal and spatial information [1] and decoding it is essential to signal processing especially in the area of image processing. However, an important and often difficult aspect of manipulating the phase signal is the wrapping due to its periodical nature which can introduce mathematical discontinuities. Phase unwrapping techniques have been developed to restore the "continuous" phase from its wrapped version and have been studied widely in various settings such as interferometric synthetic aperture radar (InSAR) [2], [3] and MRI image processing [4], [5]. In InSAR phase data processing, investigations into phase unwrapping in the presence of phase singularities has received considerable attention over the last decade. Robust phase unwrapping strategies such as brunch-cut algorithm [6], [7] and minimum cost flow (MCF) algorithm [8]–[11] among others [12], [13] have been developed to account for the effect of these phase singularities in static 2-D phase maps.

Another area of investigation involving phase unwrapping and phase singularities stems from the study of nulls in wave scattering problems. Scattering nulls refer to the spatial locations where the amplitude of the field goes to zero, rendering the associated phase unspecified. Nye and Berry performed an early systematic study of this phenomenon in optical scattering problems [14]. It has been similarly discussed under different labels such as wave dislocations [14], phase singularities [15] and optical vortices [16]–[18] in various publications where its curious relationship to phase unwrapping has received the majority of attention. The equivalence of a discrete scattering null and phase singularity was demonstrated by Fried and Vaughn [19] while the evolution and structure of these nulls have been investigated by several researchers [15], [20], [21].

Our interest in phase unwrapping and scattering nulls is motivated by the utilization of the unwrapped phase in our iterative reconstruction algorithm for microwave medical imaging. Microwave tomographic imaging [22] is targeted at recovering dielectric properties, i.e. the permittivity and conductivity, by interrogating targets with microwave signals and utilizing the measured response to estimate the property distribution. Microwave imaging is a potentially promising alternative to traditional medical modalities because it is non-ionizing and the biological tissue can present far greater normal/malignant property contrasts [23]. Over the past decade, our studies on microwave imaging have focused on breast cancer detection [24] and thermotherapy monitoring [25]. A log-magnitude phase form (LMPF) image reconstruction algorithm was initially proposed by Meaney *et al.* [26] and demonstrated improved performance in both convergence behavior and image quality compared with a more traditional complex-valued representation. However, as we applied the LMPF algorithm in a broad range of clinical situations, we observed that it failed under certain circumstances and produce noisy or diverged results. We subsequently found that the failure of the LMPF algorithm in these situations was associated with the presence of scattering nulls within the imaging domain. In some cases, the nulls were only present in intermediate numerical solutions

EDICS: 3-RADR Radar Imaging, 2-SEQP Image Sequence Processing

*Qianqian Fang is with Thayer School of Engineering, Dartmouth College, Hanover, NH 03755 U.S.A.(phone: 617-726-9332; fax: 617-726-7422; e-mail: qianqian.fang.th05@alum.dartmouth.org).

Paul M. Meaney is with Thayer School of Engineering, Dartmouth College, Hanover, NH 03755 U.S.A.(e-mail: paul.m.meaney@dartmouth.edu).

Keith D. Paulsen is with Thayer School of Engineering, Dartmouth College, Hanover, NH 03755 U.S.A.(e-mail: keith.d.paulsen@dartmouth.edu).

computed during the Gauss-Newton iterative reconstruction process. In order to fully exploit the potential advantages of the LMPF reconstruction, mathematical analysis of the phase unwrapping phenomenon is required to ensure correct processing of the scattering nulls. Importantly, the analysis is quite general and has broad implications for several areas of interest where the spatial distribution of the signal phase is involved including microwave tomographic imaging, MRI and InSAR.

This paper is comprised of three closely related topics. First, we develop a mathematical framework for the phase unwrapping analysis. Conclusions from both complex analysis and the field of topology are utilized to formalize the phase unwrapping properties in mathematical terms. The concept of static and dynamic phase unwrapping problems are introduced to facilitate the application of the phase analysis theory. In contrast to the previous topic, we investigated the phenomenon of scattering nulls in the microwave scattering problem from a physical perspective as a natural extension of its optical counterpart. The relationship of these phase unwrapping problems in 2-D and 3-D spaces are also briefly discussed. The last topic focuses on the application of the two preceding analyses in microwave image reconstruction utilizing LMPF algorithm. Simple and robust unwrapping strategies are proposed to solve the challenges associated with the current algorithm. Image reconstructions utilizing simulated and clinical measured data are performed to test the validity and efficiency of these analyses and strategies.

II. A Mathematical Framework of Phase Unwrapping

This section is dedicated to constructing a mathematical framework for phase unwrapping. We first summarize several basic concepts, including the phase function, single-valued interval and unwrapping path from which the definition of a phase unwrapping integral (Definition 2.1) is provided. We subsequently discuss the properties of this integral with respect to single-valued intervals and path partitions (Lemmas 2.2 to 2.5), which lead to the uniqueness (Theorem 2.6) of the phase unwrapping integral. The discussions of closed path integrals (Theorem 2.8 and 2.9) yield similar conclusions to those from the complex analysis. These conclusions are further extended to $\mathbb{R}^n$ space (Theorem 2.10) in Section II-D and sampled phase field in Section II-E. Finally, the previous analysis is summarized as static phase unwrapping (Definition 2.11) to distinguish it from the more troublesome problem of dynamic phase unwrapping (Definition 2.12) where a sequence of phase maps is analyzed.

A. Phase function and the single-valued interval

In these derivations, functions with domain X and range in Y are denoted by $W : X \to Y$. More specifically, if W is a complex-valued function over n-dimensional Euclidean space, where $X = \mathbb{R}^n$ and $Y = \mathbb{C}$, one can write W in the form of $W(r) = u(r) + jv(r) = (u(r), v(r))$ where $r \in \mathbb{R}^n$ and $j = \sqrt{-1}$. If real functions $u(r)$ and $v(r)$ are both continuously differentiable in $\mathbb{R}^n$, W is said to be continuously real-differentiable [27], and consequently continuous.

Applying Euler's formula, W can also be written in exponential form:

$$W(r) = \rho(W(r)) \exp(j\Phi(W(r))) \tag{1}$$

where $\rho : \mathbb{C} \to \mathbb{R}^+ \cup \{0\}$ (a map from the complex plane to non-negative real axis) is the amplitude function and $\Phi : \mathbb{C} \to \mathbb{R}$ is the phase function. Particularly, for a complex number $w = (u, v) \in \mathbb{C}$, the phase function $\Phi(w)$ can be written as

$$\Phi(w) = \operatorname{atan}_2(v, u) + 2n\pi \tag{2}$$

where $n \in \mathbb{Z}$ is an arbitrary integer due to the periodic nature of the complex exponential function. Function atan_2 is defined as an extension of the $\arctan$ function by:

$$\operatorname{atan}_2(v, u) = \begin{cases} \arctan(v/u) & u > 0 \\ \pi \times \operatorname{sign}(v) + \arctan(v/u) & u < 0 \\ \pi/2 \times \operatorname{sign}(v) & u = 0, v \neq 0 \\ \text{arbitrary} & u = 0, v = 0 \end{cases} \tag{3}$$

where $\operatorname{sign}(v)$ is the left-side-continuous sign function of v, defined as $\operatorname{sign}(v) = 1$ if $v > 0$, -1 if $v \leq 0$.

From (2) we see that $\Phi(W(r))$ is a multi-valued real function. To simplify the analysis, we define the single-valued interval S for any given real number $\varphi_0 \in \mathbb{R}$ as $S = [\varphi_0, \varphi_0 + 2\pi)$. For any $r \in \mathbb{R}^n$ if $(u(r), v(r)) \in \mathbb{C}\backslash\{0\}$ (the $\mathbb{C}$ plane punctured at the origin, $\mathbb{C}\backslash\{0\}$ is also denoted as $\mathbb{C}^\times$), there exists one and only one integer $n_S \in \mathbb{Z}$ that satisfies (as a direct consequence of the Pigeonhole principle [40])

$$\operatorname{atan}_2(v(r), u(r)) + 2n_S\pi \in S$$

As a result, we define a single-valued function

$$\phi_S(W(r)) = \operatorname{atan}_2(v(r), u(r)) + 2n_S\pi \in S \tag{4}$$

where $\phi_S(W(r))$ is called the single-valued branch of $\Phi(W(r))$ over interval S. For convenience, we denote interval $[-\pi, \pi)$ as S_*. For any $W(r) \in \mathbb{C}^\times$, the output of function $\operatorname{atan}_2(v, u)$ always resides within S_*; therefore, (4) can be written as

$$\phi_S(W(r)) = \phi_{S_*}(W(r)) + 2n_S\pi \in S \tag{5}$$

B. Path and Phase unwrapping integral

Before defining the phase unwrapping integral, we must examine another important concept: the path or curve. In complex variable analysis, a path is defined as a continuous map between the real interval $I = [0, 1]$ to a metric space Y [27]. For example, a path in $\mathbb{C}$ is denoted as $\gamma : I \to \mathbb{C}$. $\gamma(0)$ and $\gamma(1)$ designate the initial and the terminal points of path γ. If $\gamma(0) = \gamma(1)$, γ is a closed path. A path-sum is defined as $\gamma = \sum_{i=1}^{N} \gamma_i$ with overlapping at the terminal point of γ_μ and the initial point of $\gamma_{\mu+1}$ ($1 \leq \mu < N$). A path γ is said to be piecewise continuously differentiable if it can be written as a finite path-sum of continuously differentiable paths [27]. Let $\Gamma : I \to \mathbb{R}^n$ be a piecewise continuously differentiable path and $W : \mathbb{R}^n \to \mathbb{C}$ be a continuously real-differentiable function, then for any $r \in \Gamma$, if $W(r) \neq 0$, Γ

is called a piecewise unwrappable path. Since the definition of the phase unwrapping integral involves the gradient of the phase function, we will only consider piecewise unwrappable paths throughout the rest of the paper.

Given a single-valued interval $S = [\varphi_0, \varphi_0 + 2\pi)$ and a real-differentiable function $W : \mathbb{R}^n \to \mathbb{C}$, $\Gamma : I \to \mathbb{R}^n$ is called an unwrappable path of S under W if for all $r \in \Gamma$

$$\phi_S(W(r)) \in S \backslash \{\varphi_0\} \tag{6}$$

We denote $\Gamma \in P(S, W)$, where $P(S, W)$ is the set of all unwrappable paths of complex function W over single-valued interval S. $\phi_S(W(r))$ is a composite map as $\phi_S \circ W \circ \Gamma : I \to \mathbb{R}$ which is readily shown to be piecewise continuously differentiable over I if $\Gamma \in P(S, W)$. For the identity map $\mathrm{Id} : \mathbb{C} \to \mathbb{C}$, any path in the $\mathbb{C}$ plane that does not cross phase branch cut $\phi_S(z) = \varphi_0$ and the origin is an unwrappable path.

The previous discussion sets the stage for defining the phase unwrapping integral as:

Definition 2.1 (Phase Unwrapping Integral): Let $W : \mathbb{R}^n \to \mathbb{C}$ be a continuously real-differentiable function, and $\Gamma : I \to \mathrm{dom}(W)$ be a path in the domain of W. The phase unwrapping integral of W over path Γ is then defined as

$$\int_\Gamma \nabla\phi(W(r)) \cdot \mathbf{dl} = \sum_{i=1}^{N} \int_{\Gamma_i} \nabla\phi_{S_i}(W(r)) \cdot \mathbf{dl} \tag{7}$$

where $r \in \mathbb{R}^n$, $\Gamma = \sum_{i=1}^{N} \Gamma_i$ and $\Gamma_i \in P(S_i, W)$. $\nabla\phi_{S_i}(W(r))$ is the gradient of the single-valued phase function with single-valued interval S_i.

Γ_i is called a segment of Γ, and set $\{\Gamma_i\}_{i=1}^N$ is a segmentation of path Γ. All (Γ_i, S_i) pairs comprise a set of $\{(\Gamma_i, S_i)\}_{i=1}^N$ and are referred to here as a partition of Γ (sometimes the index limits can be omitted). $Q(\Gamma)$ is used to designate the set of all partitions of Γ. For simplicity, the left-hand-side of (7) can be denoted as $\mathcal{U}(W(r), \Gamma)$ or $\mathcal{U}(W(r), \{\Gamma_i, S_i\})$.

Here, we provide a constructive proof on the existence of a partition for any piecewise unwrappable path $\Gamma : I \to \mathbb{R}^n$. Interval I is a topology space, for $\forall t \in I$, we construct the quotient space $I/\sim$ based on equivalence map [28] with $\sim = \{t | t \in I \text{ and } \phi_{S_*}(W(\Gamma(t))) \in [-\pi, 0]\}$. Since Γ and W are continuous maps, the subspaces of quotient space $I/\sim$ are continuous subintervals of I. The subintervals satisfying map $\sim$ are closed intervals whose images under Γ are unwrappable paths with $S = [-3\pi/2, \pi/2)$. The remainders are open subintervals (except those at the two ends) where $\phi_{S_*}(W(\Gamma(t))) \in (0, \pi)$. One can add necessary boundary points to transform them into closed intervals whose images under Γ are the unwrappable paths of $S = [-\pi/2, 3\pi/2)$.

C. Properties of the phase unwrapping integral

Definition 2.1 illustrates the phase unwrapping integral for any valid partition of a unwrappable path. However, for a given path, the number of possible valid partitions is infinite. In this subsection, we shall first demonstrate the independence of the integral with respect to partitions of the path, followed by an illustration of the properties of the closed-path phase unwrapping integral.

Lemma 2.2: Let $W : \mathbb{R}^n \to \mathbb{C}$ be a continuously real-differentiable function, and S be a single-valued interval. For any unwrappable path $\Gamma : I \to \mathrm{dom}(W)$ of S with $\Gamma(0)$ and $\Gamma(1)$ being the initial and terminal points, respectively, $\mathcal{U}(W(r), \Gamma)$ can be expressed as

$$\begin{aligned} \mathcal{U}(W(r), \Gamma) &= \int_\Gamma \nabla\phi_S(W(r)) \cdot \mathbf{dl} \\ &= \phi_S(W(\Gamma(1))) - \phi_S(W(\Gamma(0))) \end{aligned} \tag{8}$$

Lemma 2.2 can be easily verified by using the fundamental theorem for line integrals [29] given the piecewise continuous differentiability of ϕ_S over I.

Lemma 2.3: Let $W : \mathbb{R}^n \to \mathbb{C}$ be a continuously real-differentiable function, S_1 and S_2 be two single-valued intervals, and $\Gamma : I \to \mathrm{dom}(W)$ be a path. If $\Gamma \in P(S_1, W)$ and $\Gamma \in P(S_2, W)$, then

$$\int_\Gamma \nabla\phi_{S_1}(W(r)) \cdot \mathbf{dl} = \int_\Gamma \nabla\phi_{S_2}(W(r)) \cdot \mathbf{dl} \tag{9}$$

Proof: Utilizing Lemma 2.2, the terms in equation (9) can be written as

$$\begin{aligned} \textstyle\int_\Gamma \nabla\phi_{S_1}(W(r)) \cdot \mathbf{dl} &= \phi_{S_1}(W(\Gamma(1))) - \phi_{S_1}(W(\Gamma(0))) \\ \textstyle\int_\Gamma \nabla\phi_{S_2}(W(r)) \cdot \mathbf{dl} &= \phi_{S_2}(W(\Gamma(1))) - \phi_{S_2}(W(\Gamma(0))) \end{aligned} \tag{10}$$

Since path Γ lies in a single-valued branch of the phase function, the change of the single-valued interval will result in simultaneous addition or subtraction of $2n\pi$ for all points in Γ. Therefore, the phase differences between $W(\Gamma(0))$ and $W(\Gamma(1))$ remain constant, and from (10), Lemma 2.3 is proven. ■

Lemma 2.4: Let $W : \mathbb{R}^n \to \mathbb{C}$ be a continuously real-differentiable function. For any path $\Gamma : I \to \mathrm{dom}(W)$, if $\{(\Gamma_i, S_i)\}_{i=1}^N \in Q(\Gamma)$, we can write

$$\mathcal{U}(W(r), \Gamma) = \sum_{i=1}^{N} \left(\phi_{S_i}(W(\Gamma_i(1))) - \phi_{S_i}(W(\Gamma_i(0)))\right) \tag{11}$$

which follows directly from Definition 2.1 and Lemma 2.2.

Lemma 2.5: Let $W : \mathbb{R}^n \to \mathbb{C}$ be a continuously real-differentiable function, $\Gamma : I \to \mathrm{dom}(W)$ be a path, and $\{(\Gamma_i, S_i)\}_{i=1}^N \in Q(\Gamma)$ be a partition of Γ. If $\Gamma_i = \sum_{j=1}^{N_i} \Gamma_{i,j}$, then $\bigcup_{i,j} \{(\Gamma_{i,j}, S_i)\} \in Q(\Gamma)$ and

$$\mathcal{U}\left(W(r), \{(\Gamma_i, S_i)\}\right) = \mathcal{U}\left(W(r), \bigcup_{i,j} \{(\Gamma_{i,j}, S_i)\}\right) \tag{12}$$

Proof: If $\Gamma_i \in P(S_i, W)$, the continuous subspaces $\Gamma_{i,j}$ are also unwrappable paths of S_i, i.e. $\Gamma_{i,j} \in P(S_i, W)$ for all j. Therefore, $\bigcup_{i,j} \{(\Gamma_{i,j}, S_i)\}$ is a valid partition of path Γ, referred to as a refinement of partition $\{(\Gamma_i, S_i)\}$. From Lemma 2.4,

$$\mathcal{U}(W(r), \Gamma_i) = \sum_{j=1}^{N_i} \left(\phi_{S_i}(W(\Gamma_{i,j}(1))) - \phi_{S_i}(W(\Gamma_{i,j}(0)))\right) \tag{13}$$

From the path-sum definition, segments $\Gamma_{i,j}$ overlap at initial and terminal points. Therefore, the phases at intermediate points cancel and the summation in (13) leaves only the phase difference between the initial and terminal points of Γ_i. ■

Theorem 2.6: Let $W : \mathbb{R}^n \to \mathbb{C}$ be a continuously real-differentiable function, $\Gamma : I \to \mathrm{dom}(W)$ be a path, and $\{(\Gamma_i^a, S_i^a)\}_{i=1}^{N_a}$ and $\{(\Gamma_i^b, S_i^b)\}_{i=1}^{N_b}$ be two partitions of Γ. Then

$$\mathcal{U}(W(r), \{(\Gamma_i^a, S_i^a)\}) = \mathcal{U}(W(r), \{(\Gamma_i^b, S_i^b)\}) \quad (14)$$

Proof: Construct a refinement $\{(\Gamma_i^c, S_i^c)\}_{i=1}^{N_c}$ of $\{(\Gamma_i^a, S_i^a)\}_{i=1}^{N_a}$, where, for $\forall \Gamma_i^c$, there exist two positive integers, $M, N \in \mathbb{N}$ with $\Gamma_i^c \subset \left(\Gamma_M^a \cap \Gamma_N^b\right)$. Letting $S_i^c = S_M^a$, from Lemma 2.5, we can write

$$\mathcal{U}(W(r), \{(\Gamma_i^c, S_i^c)\}) = \mathcal{U}(W(r), \{(\Gamma_i^a, S_i^a)\}) \quad (15)$$

Furthermore, letting $S_i^{c\prime} = S_N^b$ produces

$$\mathcal{U}(W(r), \{(\Gamma_i^c, S_i^{c\prime})\}) = \mathcal{U}(W(r), \{(\Gamma_i^b, S_i^b)\}) \quad (16)$$

From Lemma 2.3, the left-hand-sides of (15) and (16) are equal. Therefore, the associated right-hand-sides are also equivalent. ■

Since complex function W is a continuous map, the image of a piecewise unwrappable path in the range of W is also a piecewise unwrappable path. As a result, the integral variable can be transformed to the $\mathbb{C}$ plane:

Lemma 2.7: Let $W : \mathbb{R}^n \to \mathbb{C}$ be a continuously real-differentiable function, and $\Gamma : I \to \mathrm{dom}(W)$ be a path. Let $\mathrm{Id} : \mathbb{C} \to \mathbb{C}$ be an identity map over $\mathbb{C}$, and Γ' be the image of Γ under map W, i.e. $W : \Gamma \to \Gamma'$. Then

$$\mathcal{U}(W(r), \Gamma) = \mathcal{U}(\mathrm{Id}(z), \Gamma') \quad (17)$$

Proof: Utilizing a partition of Γ, $\{(\Gamma_i, S_i)\}$, from Lemma 2.4 , we can write

$$\mathcal{U}(W(r), \{(\Gamma_i, S_i)\}) = \sum_i \left(\phi_{S_i}(W(\Gamma_i(1))) - \phi_{S_i}(W(\Gamma_i(0)))\right) \quad (18)$$

For any segment Γ_i, the image in $\mathbb{C}$ under W is Γ_i' and $\Gamma' = \sum_i \Gamma_i'$. Since $\Gamma \in P(S_i, W)$, $\Gamma_i' \in P(S_i, \mathrm{Id})$. Consequently, $\{(\Gamma_i', S_i)\}$ is a partition of path Γ'. From Lemma 2.4

$$\mathcal{U}(\mathrm{Id}(r), \{(\Gamma_i', S_i)\}) = \sum_i \left(\phi_{S_i}(\mathrm{Id}(\Gamma_i'(1))) - \phi_{S_i}(\mathrm{Id}(\Gamma_i'(0)))\right) \quad (19)$$

Recognizing $\Gamma_i'(0) = W(\Gamma_i(0))$, $\Gamma_i'(1) = W(\Gamma_i(1))$ and $Id(z) = z$, Lemma 2.7 is proven. ■

The phase unwrapping integral over a closed path possesses similarities to that of the complex integral. The following two theorems are useful in real applications.

Theorem 2.8: Let $W : \mathbb{R}^n \to \mathbb{C}$ be a continuously real-differentiable function, and $\Gamma : I \to \mathrm{dom}(W)$ be a closed path, and $\Gamma' \subset \mathbb{C}$ be the image of Γ. If Γ' does not enclose $z = 0$ in the $\mathbb{C}$ space, we can write

$$\mathcal{U}(W(r), \Gamma) = 0 \quad (20)$$

Proof: From Lemma 2.7, we produce $\mathcal{U}(W(r), \Gamma) = \mathcal{U}(\mathrm{Id}(r), \Gamma')$. The closed path integral $\mathcal{U}(\mathrm{Id}(r), \Gamma')$ in $\mathbb{C}$ space is subsequently discussed in two cases:

1. If there exists a real number, φ_0, making $\Gamma' \in P(S, \mathrm{Id})$ where $S = [\varphi_0, \varphi_0 + 2\pi)$, because phase map ϕ_S is a continuous function over Γ', from the extreme value theorem [28], there must exist two points $z_A, z_B \in \Gamma'$, where $\phi(z_A) = \sup(\phi_S(\Gamma')) = \phi_H$ and $\phi(z_B) = \inf(\phi_S(\Gamma')) = \phi_L$ (Fig. 1 a). z_A and z_B divide Γ' into two segments Γ_{AB}' and Γ_{BA}' both of which are unwrappable paths of S. From Lemma 2.2, the summation of the phase unwrapping integral over the two paths is zero.

2. If such φ_0 does not exist (Fig. 1 b), pairs of opposing paths along the u and v axes between the intersections with Γ' are added. This creates a collection of closed curves with each covering a single quadrant. Therefore, the conclusion from case 1 can be applied here to produce zeros for all paths. ■

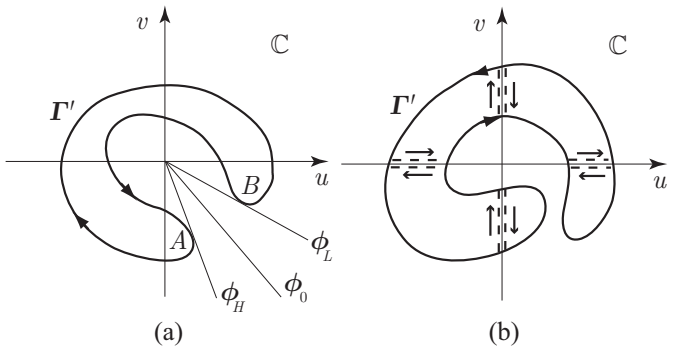

Fig. 1. Illustration of the phase integral as discussed in Theorem 2.8 (a) case 1, and (b) case 2

Theorem 2.8 can be extended if the concept of the winding number or index [27] from topology is incorporated to produce

Theorem 2.9: Let $W : \mathbb{R}^n \to \mathbb{C}$ be a continuously real-differentiable function, $\Gamma : I \to \mathrm{dom}(W)$ be a closed path, Γ' be the image of Γ in $\mathbb{C}$, and $\mathrm{Ind}_{\Gamma'}(0)$ be the winding number of closed path Γ' with respect to the origin in $\mathbb{C}$. Then

$$\mathcal{U}(W(r), \Gamma) = 2\pi \cdot \mathrm{Ind}_{\Gamma'}(0) = \frac{1}{j} \oint_{\Gamma'} \frac{dz}{z} \quad (21)$$

Proof: 1. If $\mathrm{Ind}_{\Gamma'}(0) = 0$ (i.e. closed path Γ' does not enclose the origin in $\mathbb{C}$), Theorem 2.9 is proven by Theorem 2.8.

2. If $\mathrm{Ind}_{\Gamma'}(0) = 1$, we create a rectangular mesh within Γ' by adding opposite paths along the grid lines (as shown in Fig. 2). The integral over Γ' is converted into a summation of closed path integrals along the boundary of each subdivided zone. The closed paths fully within Γ' are all rectangular, while those sharing the boundary of Γ' are comprised of some straight lines within Γ' and the curved line segments along associated subsections of Γ'. Because the directions of integration along any one straight line segment are opposite to each other for adjacent subzones sharing that line segment, all internal line integrations within Γ' cancel. Only one rectangle Γ_R' encloses the origin while the integrals for the remaining closed paths yield zeros from Theorem 2.8. Denoting the two intersections of Γ_R' with the u-axis by A and B, path Γ_R' is broken into Γ_{AB}' and Γ_{BA}'. Choosing $S_1 = [-\pi/2, 3\pi/2)$ and $S_2 = [\pi/2, 5\pi/2)$ where $\Gamma_{AB}' \in P(S_1, \mathrm{Id})$ and $\Gamma_{BA}' \in P(S_2, \mathrm{Id})$, we produce

$$\begin{aligned} \mathcal{U}(\mathrm{Id}(z), \Gamma_R') &= \mathcal{U}(\mathrm{Id}(z), \Gamma_{AB}') + \mathcal{U}(\mathrm{Id}(z), \Gamma_{BA}') \\ &= (\pi - 0) + (2\pi - \pi) = 2\pi \end{aligned} \quad (22)$$

For paths with $\mathrm{Ind}_{\Gamma'}(0) = -1$, the analysis is similar.

3. if $|\mathrm{Ind}_{\Gamma'}(0)|$ is larger than 1, such as in Fig. 3, we can always add pairs of paths along the u-axis between its

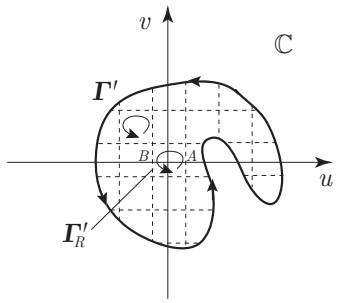

Fig. 2. Closed path integral over Γ' with $\mathrm{Ind}_{\Gamma'}(0) = 1$ illustrating the rectangular segmentation of the enclosed area utilized for demonstrating case 2 in Theorem 2.9

intersections with path Γ', resulting in a collection of enclosed paths Γ'_i with $\mathrm{Ind}_{\Gamma'_i}(0) = \pm 1$. From the discussion above and the additive property of winding numbers [27], Theorem 2.9 is readily proven.

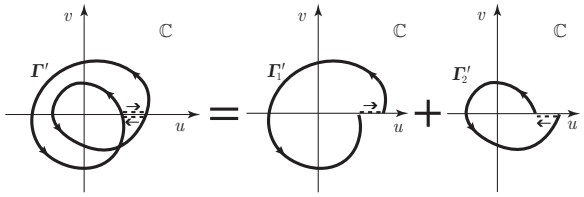

Fig. 3. Decomposition of a multi-winded closed path into simple closed paths with winding number of ± 1

■

D. Closed path phase unwrapping integral in $\mathbb{R}^n$ space

The conclusions in the previous section are general for any continuously real-differentiable complex function over $\mathbb{R}^n$. Notice that Theorems 2.8 and 2.9 specifically involve the image of the unwrapping path in $\mathbb{C}$ space, while in many real-world applications, the unwrapping paths are chosen directly in $\mathbb{R}^n$ space (more specifically, in $\mathbb{R}^2$ or $\mathbb{R}^3$). An extension of Theorem 2.9 from $\mathbb{C}$ to $\mathbb{R}^n$ space is essential for such cases.

In $\mathbb{R}^n$ space, the complete inverse image of $z = 0 \in \mathbb{C}$ is defined as the point set $\{r | r \in \mathbb{R}^n, W(r) = 0\}$, denoted by $W^{-1}(0)$. Equivalently, $W^{-1}(0)$ can be defined as the solution of

$$\begin{cases} u(r) = 0 \\ v(r) = 0 \end{cases} \qquad r \in \mathbb{R}^n \tag{23}$$

where $u(r)$ and $v(r)$ are the real and imaginary part of W, respectively.

Assuming map $W : \mathbb{R}^n \to \mathbb{C}$ has full rank over every point in $W^{-1}(0)$, from Theorem 5.8 and Corollary 5.9 of [38], $W^{-1}(0)$ will be a closed regular submanifold with dimension $n-2$. Instead of studying the topological relationship between Γ' and $z = 0$ in $\mathbb{C}$ as was the case in Theorem 2.9, we can investigate the reciprocal graph pair, i.e. Γ and $W^{-1}(r)$, in $\mathbb{R}^n$ space since both are closed regular manifolds. In higher dimensional spaces, the corresponding concept to the winding number is the linking number [30], [31]. In such cases, it is not difficult to prove from the definition that the following is true

$$\mathrm{Ind}_{\Gamma'}(0) = \mathrm{Lk}(\Gamma, W^{-1}(0)) \tag{24}$$

where $\mathrm{Lk}(\Gamma, W^{-1}(0))$ is the linking number between the unwrapping path Γ and the complete inverse image of $z = 0$.

Consequently, we can state the following conclusion:

Theorem 2.10: Let $W : \mathbb{R}^n \to \mathbb{C}$ be a continuously real-differentiable function with $n \geq 2$, and $\Gamma : I \to \mathrm{dom}(W)$ be a closed path. If W has full rank at every point in $W^{-1}(0) = \{r | r \in \mathbb{R}^n, W(r) = 0\}$, then

$$\mathcal{U}(W(r), \Gamma) = 2\pi \cdot \mathrm{Lk}(\Gamma, W^{-1}(0)) \tag{25}$$

Theorem 2.10 illustrates a more realistic view of phase unwrapping over closed paths which amounts to 2π multiplied by the linking number between the chosen path and $W^{-1}(0)$. $W^{-1}(0)$ is sometimes referred to as the phase singularity. In two dimensional space, $W^{-1}(0)$ is a set of oriented point pairs such as shown in Fig. 4 a, where the cross and circle denote the locations and orientations of the phase singularities (note that the crosses and circles are always in pairs since $W^{-1}(0)$ is a closed oriented manifold); In $\mathbb{R}^3$, $W^{-1}(0)$ manifests itself as an oriented closed curve (Fig. 4 b) or set of curves, or even more complicated geometries [39]. Interestingly, Cusack [41] and Huntley [43] independently proved the phase singularities in 3D space are in the shape of a "loop". Their discovery agrees with the "closeness" property of $W^{-1}(0)$ identified in the above derivations.

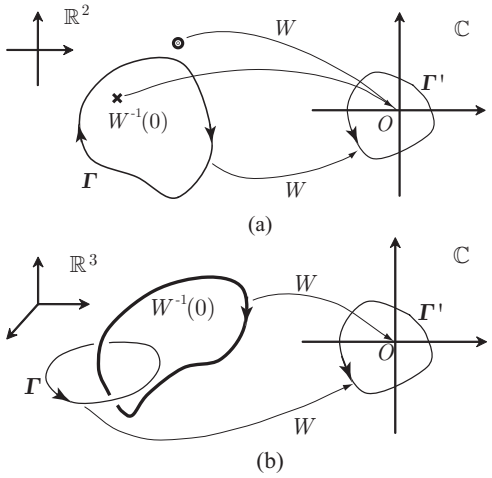

Fig. 4. Mapping relationships between (a) $\mathbb{R}^2$ or (b) $\mathbb{R}^3$ space and $\mathbb{C}$. The cross and circle in $\mathbb{R}^2$ and bolded line in $\mathbb{R}^3$ are the pre-images of the origin in $\mathbb{C}$.

E. Phase unwrapping over a sampled phase field

To this point, we have focused on the properties of phase unwrapping integral over continuous phase fields. However, phase unwrapping over sampled phase fields, especially on a regular grid, is of particular practical importance. Multiple approaches have been proposed for efficiently unwrapping sampled phase fields from InSAR, MRI and optical interferometry measurements [6], [7], [9], [12].

For the sampled phase field, a frequently used notation is "phase error" [42], [43], defined as

$$\Delta\phi(\Gamma) = \sum_{k=1}^{N_\Gamma} \text{round}\{(\phi_{S*}(\Gamma_k(1)) - \phi_{S*}(\Gamma_k(0)))/(2\pi)\} \tag{26}$$

where Γ is a closed path over the sampling grid, N_Γ is the number of straight segments on the path, $\phi_{S*}(\Gamma_k(0))$ and $\phi_{S*}(\Gamma_k(1))$ are the wrapped phases at the initial and terminal points of the k-th segment of Γ, respectively, and the function $round$ denotes rounding to the closest integer.

Shannon's theorem for phase unwrapping over sampled grids is straightforward: the continuous form phase unwrapping integral (Definition 2.1) evaluated at any given path segment on the sampling grid should not exceed $(-\pi, \pi)$. Given a sampling grid satisfying Shannon's theorem, the phase error calculated by (26) essentially counts the signed intersections of the phase branch cuts for the selected path and is eventually equal to the negative of the path winding number. For 2D rectangular grids [42], there should be no more than one net phase singularity being enclosed, otherwise, Shannon's theorem is violated. The proof is clear: if there is more than one net singularity enclosed by a square path, the absolute value of the phase unwrapping integral over the path is greater than or equal to 4π; therefore, at least one of the four edges has absolute unwrapped phase greater than or equal to π which is not allowed by Shannon's theorem. Analogously, a hexagonal grid would accommodate up to two net singularities. Several examples are shown in Fig. 5 to illustrate the similarities between phase error and the phase unwrapping integral.

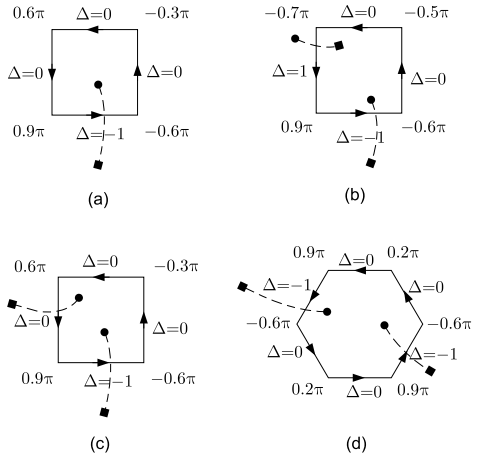

Fig. 5. Comparisons between phase error and the phase unwrapping integral for a sampled field: (a) $\sum \Delta = -1$, $\mathcal{U}(\Gamma) = 2\pi$; (b) $\sum \Delta = 0$, $\mathcal{U}(\Gamma) = 0$; (c) $\sum \Delta = -1$, $\mathcal{U}(\Gamma) = 4\pi$, Shannon's theorem is violated at the left edge and (d) $\sum \Delta = -2$, $\mathcal{U}(\Gamma) = 4\pi$. The dashed line denotes a branch cut between a positive singularity (solid circle) and a negative singularity (solid square). The numbers at the corners of each path are the wrapped phases with respect to a single value interval $[-\pi, \pi)$.

F. Static and dynamic phase unwrapping problems

In general, there are two classifications for applications of the phase unwrapping integral. The first involves only one static distribution of the complex field (in 2-D or 3-D) requiring the evaluation of the phase unwrapping integral at given field points with respect to specified reference positions. We refer to this as the static phase unwrapping problem. From Theorem 2.6, the phase unwrapping integral is unambiguously defined for any valid unwrapping path. Consequently, the static phase unwrapping problem can be simplified to:

Definition 2.11 (Static Phase Unwrapping): Let $W(r) = u(r)+jv(r)$, with $r \in D \subset \mathbb{R}^n$, be a complex field distribution over domain D. The observation set consists of a finite number of field points $\{r_i \in D\}_{i=1}^N$. For each observation point r_i, a reference field point $r_i^0 \in D$ and a piecewise unwrappable path $\Gamma_i : I \to D$ from r_i^0 to r_i is selected. The phase unwrapping integrals for all paths yield the associated unwrapped phases $\{\mathcal{U}(W(r), \Gamma_i)\}_{i=1}^N$.

Quite often, a single reference field point $r^0 \in D$ is used for all observation locations. In this case, all unwrapping paths Γ_i share a common initial point r^0. From Theorem 2.6 and 2.9, if there are no phase singularities within the complex field distribution $W(r)$ over domain D, the results of the phase unwrapping integrals are independent of the unwrapping paths and unique solutions are produced for all observation points in domain D. However, when phase singularities appear in domain D, unwrapped phases at the observation points are no longer unique. In order to generate meaningful phase information, unwrapping path selection criteria must be imposed (discussed in more detail in the following paragraphs and in Sections V and V-A).

The second type of phase unwrapping problem involves a sequence of complex field distributions governed by a set of parameters p, denoted by $\{W(r, p(t))|r \in D\}_{t=1}^{N_t}$, where parameter p is either a scalar or vector valued function of the index variable, t. In such cases, it is often essential to unwrap the phases at observation points for the complete sequence of complex fields while imposing additional constraints such as continuity requirements. This is called dynamic phase unwrapping and is defined below:

Definition 2.12 (Dynamic Phase Unwrapping): Let $W : \mathbb{R}^n \times T \to \mathbb{C}$ be a differentiable function over $\mathbb{R}^n$ and parameter space T, and $\{W(r, p(t)) = u(r, p(t)) + jv(r, p(t))\}_{t=1}^{N_t}$ be a sequence of complex field distributions over $D \subset \mathbb{R}^n$ with respect to a finite parameter sequence [28], $p : \{1, 2, ..., N_t\} \to T$. For each complex field distribution (subsequently defined as a frame) in the sequence, static phase unwrapping is performed. The reference points are generally pre-determined and the unwrapping paths are constrained by the continuity condition of the sequence usually in the form of

$$\lim_{p(t)\to p(t-1)} |\mathcal{U}(W(r, p(t)), \Gamma_i) - \mathcal{U}(W(r, p(t-1)), \Gamma_i)| = 0 \tag{27}$$

which results in a sequence of unwrapped phases $\{\mathcal{U}(W(r, p(t)), \Gamma_i)\}_{i=1,t=1}^{N,N_t}$ at the observation points.

The dynamic phase unwrapping outlined in Definition 2.12 can be viewed as a special case of its static counterpart with the unwrapping performed across yet an additional dimension, in this case, time. Similarly to static phase unwrapping, in the case where none of the frames contain phase singularities for

a given set of reference points, the unwrapped phases of each frame of the sequence are uniquely determined. The continuity condition is automatically satisfied since W is a continuous function of parameter p.

In the case where phase singularities do exist in some frames of the sequence, condition (27) will play an important role in determining the unwrapped phases in those field distributions. Since $W(r,p)$ is a continuous function of both position r and parameter p, the location of a single phase singularity in $\mathbb{R}^n$ space will continuously depend on parameter p. For $\mathbb{R}^2$ space, we expect each singularity to follow a continuous curve $\Lambda : T \rightarrow D$ connecting its location from one frame to the next if presented. We call these curves the phase singularity trajectories and define the set $\{\Lambda_i\}_{i=1}^{N_s}$ as the collection of all trajectories within the sequence, with N_s denoting the total number of trajectories. Analogously, in $\mathbb{R}^3$ space, the trajectories of the phase singularities are surfaces. Note that the trajectory Λ is not simply a linear connection of the phase singularity locations in discrete successive frames, but rather a continuous map from parameter space T to $\mathbb{R}^n$ space. Once the trajectory set of a complex field distribution sequence is identified, the evaluation of the dynamic phase unwrapping problem satisfying condition (27) is more obvious. Assuming that identical reference points are used for all frames in the sequence, one useful criterion for selecting the unwrapping paths is: the phase unwrapping path Γ for any observation point r and associated reference for a given frame shall not cross the singularity trajectory set $\{\Lambda_i\}_{i=1}^{N_s}$ for the complete sequence of frames.

The rationale for this criterion is straightforward: given an observation point r and its associated reference, the unwrapping paths in frames associated with parameters p and $p+\Delta p$ are both within the complimentary space of the trajectory set in domain D, i.e. within $D\backslash\{\Lambda_i\}$. Since neither of the paths intersect the phase singularity trajectories, the region enclosed by the two paths will not contain phase singularity at any frame. As $\Delta p \rightarrow 0$, the two paths will yield the same unwrapped phases and equation (27) is satisfied. However, if one unwrapping path crosses a trajectory, there exists a frame in which the phase singularity falls inside the region enclosed by the two paths. Subsequently as $\Delta p \rightarrow 0$, the unwrapped phase difference between the two paths will approach 2π and (27) is violated.

In Section V, we will use the notion of dynamic phase unwrapping and the path selection criteria to investigate the iterative image reconstruction process in microwave imaging.

III. Scattering Nulls in Microwave Scattering Problems

Scalar or vector Helmholtz equations with associated boundary conditions are the governing equations describing the scattering phenomenon of time-harmonic electromagnetic waves [32]. The Helmholtz equation requires the existence of the second order derivatives meaning that the electric and magnetic field components solved by the equation are all continuously real-differentiable complex functions up to the continuity at internal boundaries.

Moreover, the scattering field may contain scattering nulls, where the amplitude in the complex representation of the scattering field is zero. At these nulls, the Helmholtz equation is reduced to the Laplace equation. There is a very small subset of solutions which are rank-deficient maps and satisfy

$$\begin{cases} \partial A_r/\partial x &= \alpha \partial A_i/\partial x \\ \partial A_r/\partial y &= \alpha \partial A_i/\partial y \\ \partial A_r/\partial z &= \alpha \partial A_i/\partial z \end{cases} \tag{28}$$

where A_r and A_i are the real and imaginary parts of the field components, respectively, and α is a nonzero constant. Spatially linear-varying static fields are examples of these rank-deficient cases. However, in most cases, the solutions of scattering problems are full-ranked maps. As a result, the conclusions from Section II-C and II-F can be applied here.

In this section, we will examine the phase of the scattering field of an infinitely long, lossy cylinder with an incident TM cylindrical wave to demonstrate the scattering null phenomenon and the related 2-D phase unwrapping problem. For the 3-D phase unwrapping problem, we examine the scattering field of a lossy sphere illuminated by a dipole antenna to illustrate differences in features of scattering nulls between 2-D and 3-D spaces.

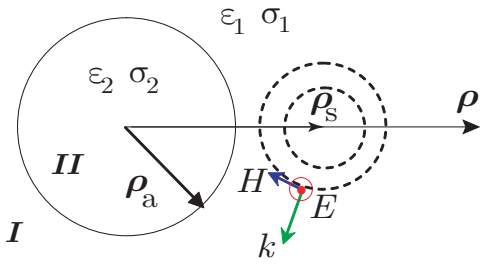

Fig. 6. Scattering of a cylindrical TM wave by an infinite cylinder

IV. Scattering nulls in 2-D problems

Consider an infinite lossy cylinder with radius ρ_a and its axis oriented along the z-axis with a line source placed in parallel to the z-axis at polar location (ρ_s, ϕ_s) (ϕ_s is zero in the configuration in Fig. 6) with current density $\vec{J} = \hat{z}\exp(j\omega t)$ (essentially a 2-D problem). The background medium has relative permittivity ϵ_1 and conductivity σ_1 with those of the cylinder being ϵ_2 and σ_2, respectively. Assuming time dependence $\exp(j\omega t)$, the complex wave number of the background and the cylinder can be written in form of $k_i = \sqrt{\omega^2\mu_0\epsilon_0\epsilon_i - \omega\mu_0\sigma_i}$, $i = 1, 2$ where ϵ_0 and μ_0 are the free space permittivity and permeability, respectively. By separating variables and matching the boundary conditions, the series solution of the E_z component can be obtained in the similar way as in [33]. The incident or primary (p), scattered (s) and total (t) E_z field distributions in region I can be written as

$$\begin{aligned} E_p^I &= E_0 \sum_{n=-\infty}^{+\infty} H_n^{(2)}(k_1\rho_>) \cdot J_n(k_1\rho_<) e^{jn(\phi-\phi_s)} \\ E_s^I &= E_0 \sum_{n=-\infty}^{+\infty} c_n \cdot H_n^{(2)}(k_1\rho_>) \cdot H_n^{(2)}(k_1\rho_<) e^{jn(\phi-\phi_s)} \\ E_t^I &= E_p^I + E_s^I \end{aligned} \tag{29}$$

while in region II, the total (t) E_z field distribution can be written as

$$E_t^{II} = E_0 \sum_{n=-\infty}^{+\infty} d_n \cdot H_n^{(2)}(k_1\rho_s) \cdot J_n(k_2\rho) e^{jn(\phi-\phi_s)} \tag{30}$$

where E_0 is the amplitude, J_n stands for the n-th Bessel function of the first kind, and $H_n^{(2)}$ for the n-th Hankel function of the second kind. $\rho_> = \max(\rho, \rho_s)$ and $\rho_< = \min(\rho, \rho_s)$. In Fig. 6, ϕ_s is simply 0. c_n and d_n are parameters defined by

$$\begin{aligned} c_n &= -\frac{k_1 J_n(k_2\rho_a) J_n'(k_2\rho_a) - k_2 J_n(k_1\rho_a) J_n'(k_2\rho_a)}{k_1 J_n(k_2\rho_a) H_n'^{(2)}(k_1\rho_a) - k_2 H_n^{(2)}(k_1\rho_a) J_n'(k_2\rho_a)} \\ d_n &= \frac{k_1 J_n(k_2\rho_a) H_n'^{(2)}(k_1\rho_a) - k_1 H_n^{(2)}(k_1\rho_a) J_n'(k_1\rho_a)}{k_1 J_n(k_2\rho_a) H_n'^{(2)}(k_1\rho_a) - k_2 H_n^{(2)}(k_1\rho_a) J_n'(k_2\rho_a)} \end{aligned}$$

When the permittivity and conductivity of the cylinder is much larger or lower than that of the background medium (i.e. high-contrast), scattering nulls will emerge in the total field. For example, in the case where the source operating frequency f=800 MHz, $\rho_a = 3$ cm, $\rho_s = 7.6$ cm, where the 0.9% saline background medium has $\epsilon_1 = 76$ and $\sigma_1 = 1.7$ S/m, and the scattering cylinder (breast fat tissue [23]) has $\epsilon_2 = 5$ and $\sigma_2 = 0.1$ S/m, the contour plot of the total field amplitude (in dB) in both regions I and II is shown in Fig. 7 (a), and that of the wrapped phase, $\phi(E_t)$, is shown in Fig. 7 (b). (The dashed white circles indicate the location and size of the scattering cylinder.) From Fig. 7, two scattering nulls (or phase singularities) can be identified where either the amplitude drops to zero and correspondingly where the phase changes abruptly. Similarly, at a higher frequency, more nulls appear both inside and outside the cylinder (Fig. 8). In this case, the electrical properties of the background and cylinder have been the previous case and the operating frequency is 2 GHz. In Fig. 8, 12 phase singularities are visible.

From a wave perspective, scattering nulls can be explained as the destructive interference points caused by the interaction of the incident and scattered waves. The nulls appear where the incident and scattered waves have equal amplitudes but $(2n+1)\pi$ phase differences. For the cylinder scattering problem shown in Fig. 8, the equal amplitude curves (Fig. 9), where $|E_p| = |E_s|$, and the out-of-phase curves, where $\phi(E_p) = \phi(E_s) + (2n+1)\pi$, are drawn and their intersections clearly indicate the locations of the nulls.

For this problem, it is quite difficult to derive a closed solution for the complex null locations. For scattering problems involving targets with complex geometries, analytical methods become impossible. In such cases, one must resort to numerical techniques, such as finite difference or finite element methods, to determine the null locations.

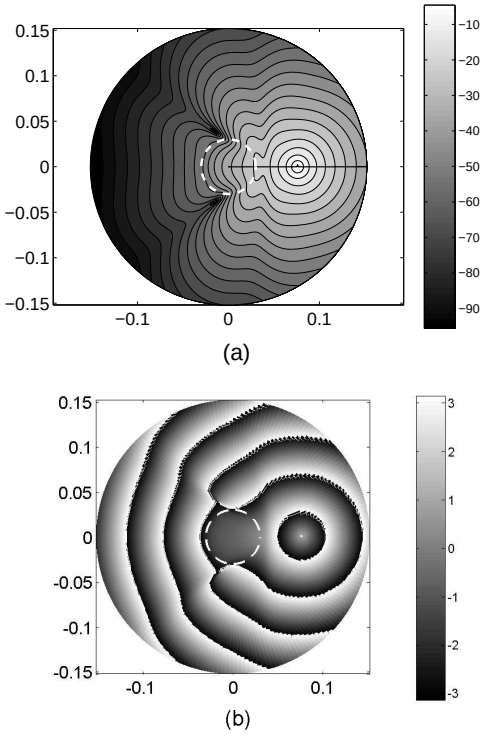

Fig. 7. Amplitude(dB) and phase(radians) plot of the total field in regions I and II at f =800 MHz.

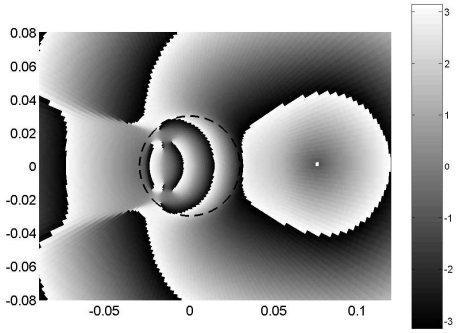

Fig. 8. Phase plot of the total field in regions I and II at f =2 GHz.

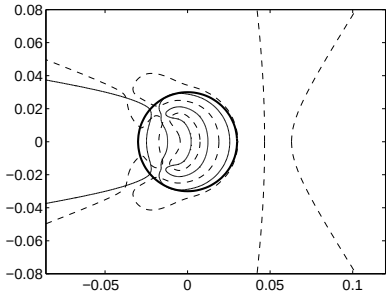

Fig. 9. Out-of-phase curves (dash lines) and equal-amplitude curves (thin solid lines) at f =2 GHz. Their intersections illustrate the scattering null locations

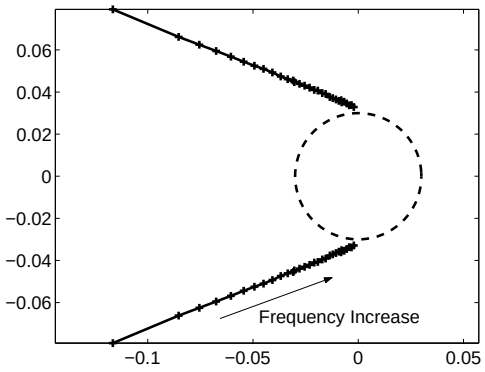

Fig. 10. The trajectories of scattering nulls for the frequency varying from 590 to 900 MHz.

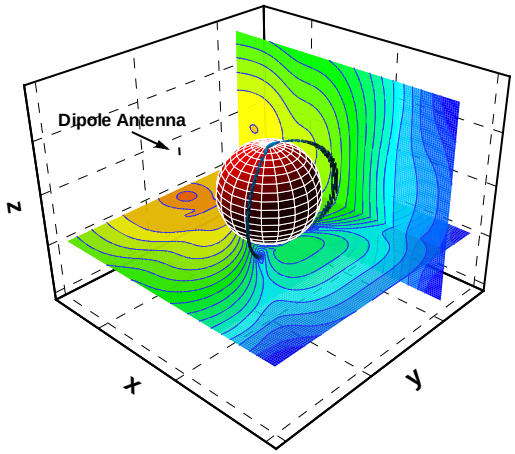

Fig. 11. 3-D scattering null in the field scattered by a lossy sphere at f =900 MHz. The ring-like null curve is on the opposite side of the sphere with respect to the short dipole antenna location.

A. Phase unwrapping for 2-D scattering fields

The static phase unwrapping problem in the previous example is relatively straightforward. Typically the source point is chosen as the zero-phase reference point. As discussed earlier, if the scattered field is null free, for any given observation point, arbitrary unwrapping paths will lead to identical solutions. However, if there are scattering nulls, the unwrapped phase will be path dependent. For example, in Fig. 7 (b), path Γ_1 and path Γ_2 yield different unwrapped phase values with a 2π phase difference.

If we take either the frequency, or the dielectric properties of either the background or cylinder, ρ_s or ρ_a of the scattered field, we can form a group of dynamic phase unwrapping problems with respect to the selected parameter. For example, if the frequency is varied from 590 to 1000 MHz in 10 MHz increments in the above problem, a sequence of electrical field distributions can be obtained. For each distribution, the locations of the nulls vary. Given the continuous nature of the scattering field, a simple linear connection between the positions of the nulls in the two successive field distributions is a relatively good approximation to the continuous trajectory of the nulls for this sequence with respect to frequency change. The approximate trajectory for the frequency sequence discussed above is shown in Fig. 10.

B. Phase unwrapping in 3-D scattering fields

In the 3-D scattering problem, the finite difference-time domain (FDTD) method was used to compute the scattering field of a lossy sphere ($\epsilon_r = 10$, $\sigma = 0.4$ S/m) for the same saline background with a dipole source illumination. The sphere was centered at the origin with radius $r_a = 3$ cm and the z-oriented dipole antenna was positioned at $(r_s, 0, \phi_s)$ with $r_s = 7.6$ cm and $\phi_s = \pi/2$ in spherical coordinates. A ring-like scattering null is extracted from the 3-D amplitude plot of the total field at 900 MHz which is shown in Fig. 11 (contour plots of the field magnitudes are also shown in the figure for two orthogonal planes).

For the dynamic phase unwrapping problem in 3-D, the phase singularity trajectories due to gradual changes in the selected parameter will form a surface, referred to as a trajectory surface. A set of unwrapping paths that does not intersect the trajectory surface will yield unambiguous unwrapped phase satisfying the continuity condition.

V. Applications of Phase Unwrapping Theory in Microwave Image Reconstruction

Iterative algorithms based on nonlinear optimizations such as distorted Born iterative method (DBIM) [32] or Gauss-Newton [34] method are widely used in microwave tomographical image reconstruction. In this type of reconstruction, the algorithm starts form an initial guess of the dielectric profile of the unknown object. The scattered fields for a range of radiating antennas are computed based on various forward field computation models, and an update of the dielectric properties is calculated from the differences between computed fields and real measurement data with gradient information. This process is repeated until the computed fields closely match the measured values. In our log-magnitude phase form (LMPF) reconstruction algorithm [26], both the complex measurement and computed field data are transformed into their amplitude and phase components. A phase unwrapping process is applied to the phase portion with respect to the transmitter reference to make it continuous and differentiable with respect to dielectric properties. Over a relatively large contrast range and large imaging targets, this algorithm exhibits faster convergence and yields superior images. However, when the target is large and the contrast is high, scattering nulls can appear in the domain. Without properly choosing the unwrapping paths, the algorithm may diverge. Even when the measured field data does not exhibit any complex null behavior, nulls can occur in the computed distributions at intermediate iteration steps. If not accounted for properly, these phase singularities can cause the algorithm to diverge to an unwanted solution.

Unwrapping the computed field phases in the Gauss-Newton iterative reconstruction approach can be regarded as a dynamic phase unwrapping problem, where the complex dielectric property $k(r)$ varies from one iteration to the next as the algorithm converges to a solution as discussed in Definition 2.12.

The continuity condition of the unwrapped phase imposed by the Gauss-Newton method requires the existence of the first order derivative:

$$\lim_{\Delta k \to 0} \frac{\|\mathcal{U}(E_z(k+\Delta k),\Gamma) - \mathcal{U}(E_z(k),\Gamma)\|}{\|\Delta k\|} < \infty \qquad (31)$$

where $||\cdot||$ denotes the l^2-norm. As a result, the conclusions from Section II-F can be applied directly to this situation. For convenience, we define the problem configuration such that the source point is always the reference point and the unwrapping paths are fixed for all measurement sites over the full set of iterations (or frames). If the unwrapping paths do not have intersections with the trajectory set associated with parameter k, then the unwrapped phases will be defined unambiguously and the continuity condition (27) is satisfied.

This strategy is relatively straightforward, however, the key to its success is developing an algorithm for effectively detecting the cross over between unwrapping path null trajectories. For 2-D or 3-D image reconstruction cases, we have devised a two-path unwrapping strategy to cope with scattering nulls associated with high-contrast scatterers. A diagram of this method in a tomographic imaging context is shown in Fig. 12. In this algorithm, we assume that the reconstruction process is initialized at a low contrast state where no nulls are present in the domain. Therefore, at the first iteration, the unwrapped phases computed from two separate paths will be identical. In all subsequent iterations, we compute the unwrapped phases $\Phi^t_{\Gamma_A}$ and $\Phi^t_{\Gamma_B}$ along path Γ_A and Γ_B. Comparing absolute differences $|\Phi^t_{\Gamma_A} - \Phi^{t-1}|$ and $|\Phi^t_{\Gamma_B} - \Phi^{t-1}|$, we choose the path corresponding to the smaller difference as the valid path and use its unwrapped phase for iteration t.

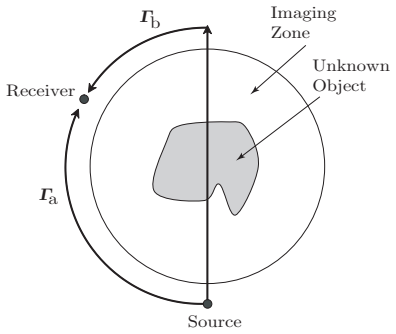

Fig. 12. Schematic plot of the two-path unwrapping strategy used in microwave tomographical imaging reconstruction.

Below, we present results utilizing both simulated and experimental (i.e. an *in vivo* breast imaging example) data. In the former, we illustrate the effectiveness when intermediate complex nulls appear in the computed forward solution. The latter illustrates a case where the algorithm has been used to reconstruct an image of a breast which was not possible without the use of the new unwrapping strategy.

A. Reconstruction with intermediate nulls

The notion of intermediate nulls refers to cases where the phase singularities do not appear in the true scattering field; however, they are created and propagate into the imaging zone during intermediate steps of the iterative reconstruction process and eventually exit the zone by the time the algorithm has converged (if it does converge to an adequate solution). During the Gauss-Newton iterative process, the reconstruction parameters do not necessarily converge monotonically. In fact, the values often overshoot the final solution and very often oscillate about the desired values until the oscillations are almost completely damped at convergence. If the unwrapped phase continuity condition is violated at intermediate steps, it could significantly alter the algorithm behavior and cause it to diverge. These types of nulls are readily processed by the two-path unwrapping strategy.

The 2-D simulation example we presented here is for a "panda face" pattern shown in Fig. 13. A 15.2 cm diameter circular antenna array consisting of 16 dipole antennas encircled the object. The imaging zone is a 14 cm diameter concentric circular region. The "panda face" is a 9 cm diameter circle with the diameters for the eyes and ears being 2.4 and 3 cm, respectively. The "panda mouth" is a quarter of a concentric annulus with an inner radius of 2.5 cm and outer radius of 3.5 cm between the angle of $-3\pi/4$ and $-\pi/4$. The electrical properties (at 1000 MHz) of the background and different zones of the "panda face" are 1) background: $\epsilon_r = 76.9$, $\sigma = 1.8(S/m)$, 2) panda face: $\epsilon_r = 55.0$, $\sigma = 1.2(S/m)$, 3) panda eyes: $\epsilon_r = 15.0$, $\sigma = 0.3(S/m)$, 4) panda ears: $\epsilon_r = 30.5$, $\sigma = 0.6(S/m)$, 5) panda mouth: $\epsilon_r = 15.0$, $\sigma = 0.3(S/m)$.

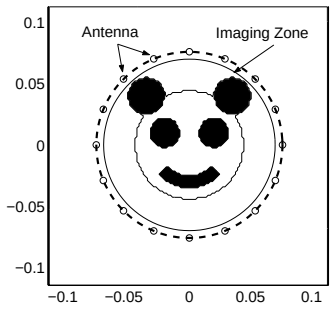

Fig. 13. Schematic diagram of the object and imaging configuration (dimensions in meters).

The measurement data was computed at 1 GHz using a 2-D finite difference-time domain (FDTD) method with a generalized perfectly matched layer (G-PML) as the absorbing boundary condition [36]. The forward solution domain was a 110×110 grid surrounded by 12 layers of G-PML. For all 16 sources, the electric fields for the exact property distribution do not contain any scattering nulls. We added noise (maximum amplitude of -100 dB and 1° phase) to the amplitude and phase data respectively, which is representative of our current hardware system [24]. The reconstruction utilized the LMPF algorithm. The reconstruction mesh conformed to the imaging zone and was comprised of 281 parameter nodes with 524 triangular elements. The Tikhonov regularization parameter, λ, was fixed at 0.05 together with our spatial filtering scheme [37] with the averaging factor set to 0.1 for stabilizing the convergence. The algorithm was initialized with a homogeneous

distribution equal to that of the background.

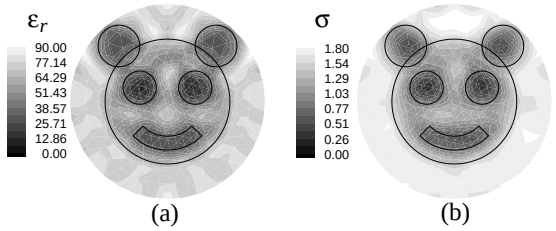

Fig. 14. Recovered dielectric profiles after 10 iterations using the two-path unwrapping strategy: (a) relative permittivity, (b) conductivity.

Using the two-path unwrapping strategy, the object was successfully reconstructed after 10 iterations with a relative electric field least squared error of 5% as shown in Fig. 14 (a) and (b). The locations, shapes and values of the features in the pattern are quite close to their true values. It is interesting to note that at the third iteration, intermediate nulls appeared in the computed field solutions for several sources and disappeared after the fourth iteration. Wrapped phase plots for the true object scattering field distribution and the forward field computed at the third iteration for a single antenna are compared in Fig. 15. Note that the scattering null migrated inside the antenna array for the third iteration (Fig. 15 b), but retreated immediately after that. Given that the unwrapping paths are usually either along the arc of the antenna or along a path through the imaging zone, phase singularities within this zone are the ones that impact the unwrapping. Without the correct phase unwrapping strategy, the reconstruction diverged quickly after the third iteration (the solution after the 10th iteration is shown in Fig. 16).

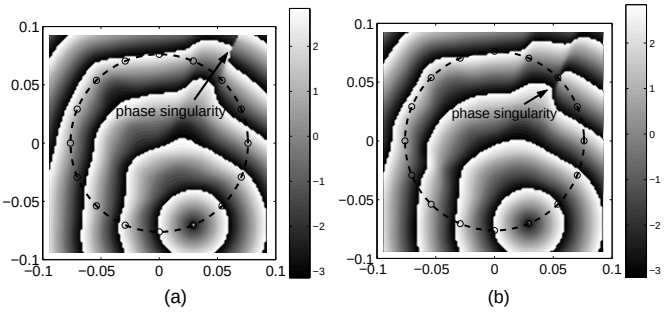

Fig. 15. Wrapped phase plots for (a) the true scattering field, (b) the forward field computed at the 3rd iteration for a single transmitter (singularity present).

B. Reconstruction of clinical measurements

The scattering nulls together with intermediate nulls are frequently encountered in the processing of measurement data from breast cancer patients especially when there are high contrast inclusions such as large tumors or cysts. Even for normal breasts, the scattered fields from the fibroglandular tissue (which has much higher water content than the predominant adipose tissue) may also induce scattering nulls. In these cases, in order to use the LMPF algorithm, we must incorporate the two-path unwrapping strategy into the reconstruction algorithm to obtain valid unwrapped phases.

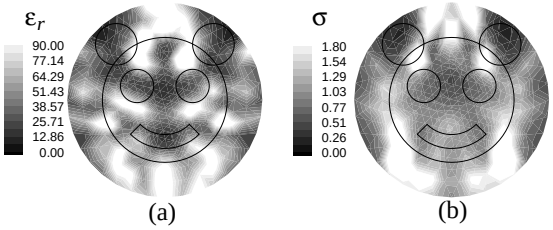

Fig. 16. Recovered dielectric profiles after 10 iterations without considering the scattering nulls: (a) relative permittivity, (b) conductivity.

In this example we reconstructed an image slice of a female breast where the subject was being treated with chemotherapy for two large malignant masses located in the upper half of the right breast near the chestwall. The measurement data was obtained with the tomographic microwave imaging system as in [24] for the plane closest to the chestwall. The reconstructed images (coronal view) at 1100 MHz utilizing the LMPF reconstruction with the two-path unwrapping strategy are shown in Fig. 17 (a) and (b). Other example images of this type are reported in [24]–[26], [36], [37]. The lower half of the images in Fig. 17 (a) and (b) show relatively low permittivity and conductivity consistent with that expected for normal breast tissue (especially adipose tissue) with a steep gradient to the perimeter of the zone corresponding to the interface with the higher property background liquid [44]. There is a large high permittivity and conductivity zone in the upper central area which is indicative of the level of property increases we would expect for tumors [45], [46]. The LMPF reconstruction without the null-detection scheme yielded images with significant artifacts as illustrated in Fig. 17 (c) and (d). The plot of relative errors [36] shown in Fig. 17 (e) further supports the assertion that the latter images are inaccurate. While the correct images are unknown, those produced using the two-path strategy are reasonably consistent with the available clinical information and are improved over the reconstruction which fails to account for phase nulls.

VI. Conclusions

In summary, we have established a general mathematical framework for explaining phase unwrapping including definitions and illustrations of particular properties related to the uniqueness and closed-path phase unwrapping. The concept of dynamic versus static phase unwrapping problems was introduced with special attention to applications in microwave imaging. These included the phenomena of scattering nulls in the high contrast and high operating frequency cases and their behavior (i.e. paths of their trajectories) as these parameters are varied.

The path selection criteria for the dynamic phase unwrapping problem was implemented in several microwave tomographical image reconstruction examples. The challenges of utilizing the LMPF algorithm were discussed from a dynamic phase unwrapping perspective and along with efficient

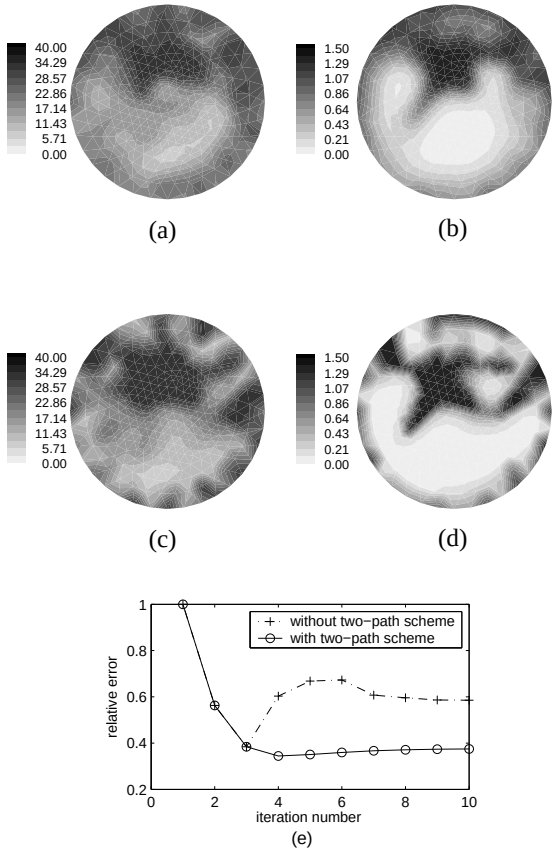

Fig. 17. Reconstructed single plane dielectric profiles representing anatomically coronal cross-sections of the breast of a cancer patient with a known malignancy in the cranial aspect near the chestwall: (a) relative permittivity with two-path unwrapping, (b) conductivity with two-path unwrapping, (c) same as (a) without two-path unwrapping, (d) same as (b) without two-path unwrapping, (e) relative error in observed versus computed field as a function of algorithm iteration number.

unwrapping strategies. The success of these reconstructions demonstrates the importance and efficiency of the our theory and analysis.

Further studies will include phase unwrapping in 3-D image reconstruction, theoretical derivations on the locations and appearance condition of scattering nulls in electromagnetic scattering problems and seeking other possible applications would help us to achieve an in-depth understanding of both phase unwrapping and scattering nulls.

VII. Acknowledgement

The authors would like to express their gratitude to professor Vladimir Chernov of the Mathematics Department of Dartmouth College for his helpful discussions in the study of topology. This work is partially supported by NIH/NCI under grant P01-C480139.

References

[1] A. V. Oppenheim, J. S. Lim, "The importance of phase in signals," In Proceedings of the IEEE, volume 69, pages 529-541, May 1981. 39

[2] H. A. Zebker, R. M. Goldstein, "Topographic Mapping from Interferometric Synthetic Aperture Radar Observations," Journal of Geophysical Research, 91, pp. 4993-4999, 1986.

[3] D. C. Ghiglia,M. D. Pritt, "Two-dimensional phase unwrapping : theory, algorithms, and software". New York: J. Wiley, 1998.

[4] R. Cusack, N. Papadakis, "New Robust 3-D Phase Unwrapping Algorithms: Application to Magnetic Field Mapping and Undistorting Echoplanar Images," *NeuroImage*, vol. 16, Part 1, July 2002, Pages 754-764.

[5] M. Jenkinson, "Fast, automated, N-dimensional phase-unwrapping algorithm", *Magnetic Resonance in Medicine*, 49 (1), pp. 193-197, 2003.

[6] R. M. Goldstein, H. A. Zebker, C. L. Werner, "Satellite Radar Interferometry: Two-Dimensional Phase Unwrapping," *Radio Science*, 23, pp. 713-720, 1988.

[7] C. Prati, M. Giani, N. Leuratti, "SAR Interferometry: a 2-D Phase Unwrapping Technique Based on Phase and Absolute Value Informations," IGARSS '90, pp. 2043-2046, 1990.

[8] R. K. Ahuja, T. L. Magnanti, and J. B. Orlin, *Network Flows: Theory, Algorithms, and Applications*. Englewood Cliffs, NJ: Prentice-Hall, 1993.

[9] M. Costantini, "A Novel Phase Unwrapping Method Based on Network Programming," *IEEE Trans. on Geoscience and Remote Sensing*, vol. 36, No. 3, May 1998.

[10] A. Refice, G. Satalino, S. Stramaglia, M. Chiaradia, and N. Veneziani, "Weights determination for minimum cost flow InSAR phase unwrapping," in *Proc. IGARSS*, Hamburg, Germany, pp. 1342-1344, 1999.

[11] G. Carballo and P. Fieguth, "Probabilistic cost functions for network flow phase unwrapping," *IEEE Trans. Geosci. Remote Sensing*, vol. 38, pp. 2192-2201, Sept. 2000.

[12] D. L. Fried, "Least-Squares Fitting a Wave-Front Distortion Estimate to an Array of Phase-Difference Measurements," *Journal of the Optical Society of America*, 67, pp.370-375, 2977, 1977

[13] O. Loffeld, R. Kramer, "Phase Unwrapping for SAR Interferometry C A Data Fusion Approach by Kalman Filtering," in *Proc. IGARSS*, Hamburg, Germany, 1999.

[14] J. F. Nye and M. V. Berry, "Dislocations in wave trains," *Proc. Roy. Soc.* Lond. A 336, 165-190, 1974.

[15] H. F. Schouten, T. D. Visser, G. Gbur, D. Lenstra, and H. Blok, "Creation and annihilation of phase singularities near a sub-wavelength slit," Opt. Express 11, 371-380, 2003.

[16] B. LutherDavies, J. Christou, V. Tikhonenko, Yu. S. Kivshar, "Optical vortex solitons: experiment versus theory," *J. Opt. Soc. Am. B* 14, 3045-3053, 1997.

[17] Yu. S. Kivshar, J. Christou, V. Tikhonenko, B. Luther-Davies, L. M. Pismen, "Dynamics of optical vortex solitons," *Opt. Commun.* 152, 198-206, 1998.

[18] D. Neshev, A. Nepomnyashchy, Yu. S. Kivshar, "Nonlinear Aharonov-Bohm scattering by optical vortices," *Phys. Rev. Lett.* 87, 043901-4, 2001.

[19] D. L. Fried, J. L. Vaughn, "Branch cuts in the phase function," Applied Optics 31(15), pp. 2866–2882, 1992.

[20] M. R. Dennis, "Local phase structure of wave dislocation lines: twist and twirl," *Journal of Optics A: Pure and Applied Optics*, special issue on singular optics, Apr. 2004.

[21] J. F. Nye, "Unfolding of higher-order wave dislocations," J. Opt. Soc. Am. A, Vol. 15, No. 5, May 1998

[22] L. E. Larsen, J. H. Jacobi, "Microwave scattering parameter imagery of an isolated canine kidney," *Med Phys* 1979; 6:394-403

[23] R. Pethig, "Dielectric properties of biological materials: biophysical and medical applications," *IEEE Transactions on Electrical Insulation*, vol. 19, pp. 453-474, 1984.

[24] P. M. Meaney, M. W. Fanning, D. Li, S. P. Poplack, K. D. Paulsen, "A clinical prototype for active microwave imaging of the breast," *IEEE Trans. Microwave Theory and Tech.*, vol. 48, pp. 1841-1853, 2000.

[25] P. M. Meaney, M. W. Fanning, K. D. Paulsen, D. Li, S. A. Pendergrass, Q. Fang, K. L. Moodie, "Microwave thermal imaging: Initial *in vivo* experience with a single heating zone," *International Journal of Hyperthermia*, 2003 (in press).

[26] P. M. Meaney,K. D. Paulsen, B. W. Pogue, M. I. Miga , "Microwave image reconstruction utilizing log-magnitude and unwrapped phase to improve high-contrast object recovery," *IEEE Transactions on Medical Imaging*, vol. 20, pp. 104-116, 2001.

[27] R. Remmert, *Theory of Complex Functions*, Springer-Verlag, New York, 1991.

[28] J. M. Lee, *Introduction to Topological Manifolds*, Springer-Verlag New York, 2000.

[29] C. Henry Edwards, D. E. Penney, *Multivariable calculus with analytic geometry*, Prentice-Hall, Inc, 1998

[30] L. Kauffman, *Knots and Physics*. Teaneck, NJ: World Scientific, p. 19, 1991

[31] S. P. Novikov, *Topology I: General Survey*, Springer-Verlag Berlin Heidelberg, 1996
[32] W. C. Chew, "Waves and Fields in Inhomogeneous Media," New York: Van Nostrand-Reinhold, 1990.
[33] R. F. Harrington, *Time-Harmonic Electromagnetic Fields*, New York: McGrawHill Book Company, 1961.
[34] N. Joachimowicz, C. Pichot, J. P. Hugonin, "Inverse scattering: an iterative numerical method for electromagnetic imaging," *IEEE Transactions on Antennas and Propagation*, vol. 39, pp. 1742-1752, 1991
[35] D. L. Fried, "Branch point problem in adaptive optics," J. Opt. Soc. Am. 15(10), pp. 2759–2768, 1998.
[36] Q. Fang, P. M. Meaney, K. D. Paulsen, "Microwave Image Reconstruction of Tissue Property Dispersion Characteristics Utilizing Multiple Frequency Information," *IEEE Trans. Microwave Techniques and Technology*, submitted, 2004.
[37] P. M. Meaney, E. Demidenko, N. K. Yagnamurthy, D. Li, M. W. Fanning, K. D. Paulsen, "A two-stage microwave image reconstruction procedure for improved internal feature extraction," *Med. Phys.*,, vol. 28, pp. 2358-2369, 2001.
[38] W. M. Boothby, *An introduction to differentiable manifolds and Riemannian Geometry*, 2nd edition, Academic Press, 1986.
[39] M. V. Berry, M. R. Dennis, "Knotted and linked phase singularities in monochromatic waves," *Proc. R. Soc. A* 457 2251C63, 2001.
[40] G. Chartrand, *Introductory Graph Theory* New York: Dover, p. 38, 1985.
[41] R. Cusack, "Unwrapping 3d maps of magnetic field deviations for use in undistorting fMRI images of the brain," paper presented at the *Institute of Physics Applied Optics Divisional Conference*, Loughborough, UK, September 2000
[42] D. J. Bone, "Fourier fringe analysis: the two-dimensional phase unwrapping problem", *Applied Optics*, 30, pp. 3627-3632, 1991.
[43] J. M. Huntley, "Three-dimensional noise-immune phase unwrapping algorithm", *Applied Optics*, 40 (23), pp. 3901-3908, 2001
[44] P. M. Meaney, S. A. Pendergrass, M. W. Fanning, D. Li, and K. D. Paulsen, "Importance of using a reduced contrast coupling medium in 2D microwave breast imaging," *Journal of Electromagnetic Waves and Applications*, 17, pp. 333-355, 2003.
[45] S. S. Chaudhury, R. K. Mishra, A. Swarup and J. M. Thomas, "Dielectric properties of normal and malignant human breast tissues at radiowave and microwave frequencies," *Indian. J. Biochem. Biophys.*, vol. 21, pp. 76-79, 1984.
[46] W. T. Joines, Y. Zhang, C. Li, R. L. Jirtle, "The measured electrical properties of normal and malignant human tissues from 50 to 900 Mhz," *Med. Phys.*, vol. 21, pp. 547-50, 1994.

Qianqian Fang (S'03-M'05) was born in Anyang, Henan, China, in 1976. He received B.Eng. degree in electrical engineering from the University of Electronic Science and Technology of China (UESTC), Chengdu, Sichuan, China, in 1999, and Ph.D. degree in biomedical engineering at Thayer School of Engineering, Dartmouth College, Hanover, USA, in 2005. He is currently a research fellow at Martinos Center for Biomedical Imaging, Massachusetts General Hospital, USA.

From 1999 to 2000, he was a Research Assistant at Computational Electromagnetics Lab, UESTC, and implemented Finite Difference-Time Domain (FDTD) and absorption boundary condition for electromagnetic pulse well-logging. From 2000 to 2004, he was a Research Assistant in microwave imaging group at Dartmouth College, focusing on three-dimensional microwave imaging, FDTD technique and phase unwrapping. He has been a Postdoctoral Research Fellow at Massachusetts General Hospital since early 2005. His current research interests include diffuse optical tomography for breast cancer detection and optical-mechanical modeling of breast under compressions.

Paul M. Meaney (M'92) received A.B.'s in Computer Science and Electrical Engineering from Brown University in 1982, an M.S. in Electrical Engineering from the University of Massachusetts in 1985, and his Ph.D. in Biomedical Engineering from Dartmouth College in 1995.

He was a Postdoctoral Fellow at Dartmouth College from 1995-1996 and a NSF-NATO Postdoctoral Fellow at the Royal Marsden Hospital in Sutton, England from 1996-1997. He has been a Research Assistant Professor at Dartmouth College since 1997. His interests include developing microwave imaging for biomedical applications – especially breast imaging and hyperthermia monitoring, along with elastography and various applications of thermal modeling.

Keith D. Paulsen (S'85-M'86) received the B.S. degree in biomedical engineering from Duke University, Durham, NC, in 1981 and the M.S. and Ph.D. degrees in biomedical engineering from Dartmouth College, Hanover, NH, in 1984 and 1986, respectively.

From 1986 to 1988, he was an Assistant Professor in the Electromagnetics Group within the Department of Electrical and Computer Engineering, University of Arizona, Tucson. He is currently a Professor at the Thayer School of Engineering, Dartmouth College and the Director of the Radiobiology and Bioengineering Research Program for the Norris Cotton Cancer Center within the Dartmouth-Hitchcock Medical Center, Lebanon, NH. His research interests include computational methods with particular emphasis on biomedical problems in cancer therapy and imaging, and model-guided surgery.